Ytterbium based back-to-back Schottky diodes as light-activated MOS capacitors and high-frequency band filters for next-generation 6G applications

H. K. KHANFAR[1,*], A. F. QASRAWI[2,3], M. F. ABU ALROB[2]
[1]*Department of Computer Systems Engineering, Arab American University, Palestine*
[2]*Department of Physics, Arab American University, Jenin, Palestine*
[3]*Department of Electrical and Electronics Engineering, Istinye University, 34010, Istanbul, Turkey*

In this study, Yb/p-Si/Yb Schottky devices were fabricated by thermally evaporating Yb contacts onto p-Si substrates under high vacuum, exhibiting MOS characteristics. These devices feature tunable flat band voltage and built-in potential under illumination, with a photo-controlled cutoff frequency spanning from the microwave to the terahertz regime. Functioning as microwave band filters, they show reflection coefficient, return loss, and voltage standing wave ratio values suitable for microwave resonators. Simulation suggests that optimizing resistance and capacitance enhances the reflection coefficient, return loss, and voltage standing wave ratio, improving performance for next-generation and terahertz applications.

(Received January 17, 2025; accepted June 4, 2025)

Keywords: 6G, Photo-capacitors, Schottky barriers, Terahertz filters, Yb/p-Si

1. Introduction

Metal-semiconductor contact based devices has captured the attention of research community due to their wide range of applications [1-10]. A remarkable metal which captured the attention in this technology sector is ytterbium (Yb). Yb based devices finds applications as microwave resonators and optical wave guides operative in a spectral range that extends from microwave to optics [1]. The use of Yb as a contact is a feature because it resulted in a non-alloyed ohmic contact to some n-type semiconductors (n-GaN) [2]. Such feature is necessary to have low resistance contacts [2]. In addition, Yb is employed as a Schottky contact to enhance the performance of $Cu(In_{1-x}Ga_x)Se_2$ (CIGS) photovoltaic devices [3]. Yb/CIGS photodiodes exhibited a light to dark current ratios of 10^3 at an illumination intensity of 25 mW/cm^2 [3]. They also revealed solar cell characteristics presented by an open circuit voltage of 0.30 V and short circuit current density of 78.6 mA/cm^2 [3].

Ytterbium contacts are also used to fabricate back-to-back Schottky devices (BBS) [4]. A BBS device operates on the principle that when one side is forward biased, the other side is reverse biased. By this operation method the dark current is kept at the minimum and high asymmetry ratios are achievable [10]. BBS devices are also beneficial for the isolation of electric signals through connecting the Schottky electrodes to separate parts of electronic circuit [10]. These devices can perform as low noise amplifiers [11] and field effect transistors employable in 4G, 5G and 6G technology applications as microwave resonators or band filters [9,12]. As for examples, Yb/WO_3/Yb devices were found adequate for the fabrication of microwave resonators. The microwave cutoff frequency for this device reached 2.0 GHz and nominated the device for 4G/5G technology applications [4]. It is known that 4G, 5G, and the emerging 6G technologies represent significant advancements in wireless communication, offering faster data rates, lower latency, and increased connectivity. 4G primarily operates in the frequency range of 1-8 GHz, while 5G extends into higher frequency bands, including sub-6 GHz and millimeter-wave (mmwave) frequencies up to 100 GHz. 6G is anticipated to explore even higher frequency bands, potentially reaching into the terahertz range. These advancements enable the transmission of massive amounts of data and support applications such as augmented reality, autonomous vehicles, and the Internet of Things. Quad-band operation, on the other hand, refers to devices capable of operating across multiple frequency bands simultaneously, typically covering global system for mobile communication (GSM), universal mobile telecommunication systems (UMTS), 4G long term evolution (LTE) and 5G bands. By leveraging quad-band operation, devices can achieve seamless connectivity and better performance across diverse network environments, ensuring optimal user experience and reliability in the rapidly evolving landscape of wireless communication technologies [13].

One other remarkable Schottky devices which captured our interest is Yb/p-Si (YS). YS devices showed promising photodiode characteristics. They exhibited photovoltaic effect presented by an open circuit voltage of 0.21 V, short circuit current of 16 μA and fill factor exceeding 60% when irradiated with light of intensity of ~0.10 W/cm^2 [5]. YS devices also revealed high rectification ratios of ~10^6 [6]. High rectification ratios close to this value are used in ultrafast switching devices [6]. The functionality of the ytterbium based Schottky devices are listed in Table 1.

In the light of these smart features of the YS devices we are motivated to produce a light controlled microwave

resonators suitable for 6G and terahertz technology needs. The device is simply made of two back contacted YS diodes. The back-to-back Schottky diodes (Yb/p −Si/Yb) are tested as high frequency capacitors in the dark and under light illumination. The effect of light illumination on the capacitance-voltage characteristics and on the capacitance, resistance and cutoff frequency spectra in the frequency domain of 0.01-1.80 GHz is also studied and analyzed. In addition, the device is treated as a microwave resonator showing band filter characteristics. The parameters of the microwave resonators including the magnitude of the reflection coefficient, the return loss and the voltage standing wave ratios is discussed and analyzed.

Table 1. Yb based devices and their functionalities

Device	Functionality			Reference
Yb/n-GaN	Resistor			[2]
Yb/CIGS	Photodiodes	Solar cells		[3]
Yb/WO_3/Yb	Microwave resonator	Switching		[4]
Yb/p-Si	Photodiodes	Rectifiers	Solar Cells	[5], [6]
Yb-p-Si-Yb	Photo-MOS	Resonator	6G antenna	This work

2. Experimental details

Plasma etched commercial p-type Si wafers (Alfa Aeser 99.99%) were used as active p-layer to fabricate Yb/p-Si/Yb Schottky diodes. Wafers of sizes of ~1.0 cm^2 were cleaned by acetone in an ultrasound machine prior to the deposition of Yb substrates. As demonstrated in Fig. 1 (a), the wafers were masked then inserted into a thermal vacuum evaporator to deposit Yb contacts onto its surface. For this purpose, Yb crystal lumps (Alfa Aeser, 99.99%) were located into a heat-resistive metal tungsten boat. The evaporation cycles were handled in a NORM-600 type thermal evaporator (shown in Fig. 1 (a)) under a vacuum pressure of 10^{-5} mbar. The thickness of the Yb contacts was measured by an Inficon type STM-2 thickness monitor installed in the evaporator chamber. The evaporation cycles ended after the monitor read 0.50 μm. The dark and illuminated capacitance-voltage characteristics and the impedance spectroscopy measurements were carried out using an Agilent 4291B 0.001-1.80 GHz impedance analyzer (shown in Fig. 1 (b)). Light irradiation was actualized using a tungsten halogen globe. The light power was measured using Mastech-MS8209 radiometer.

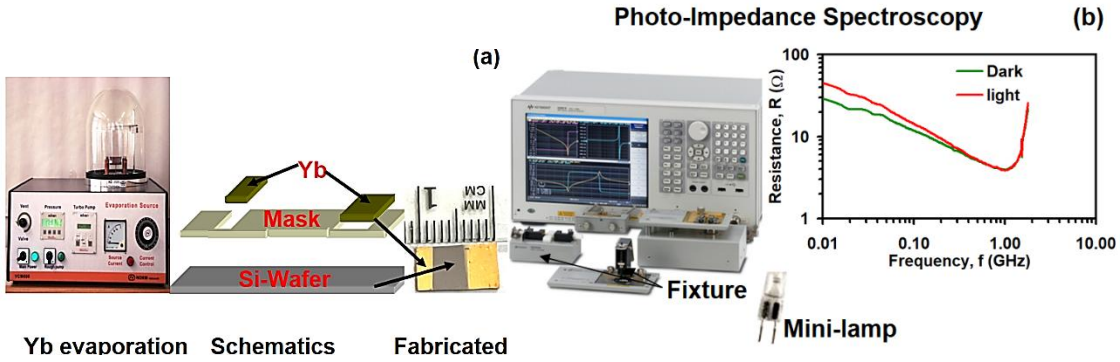

Fig. 1. (a) The schematic for producing the YSY Schottky devices. (b) The photo-impedance spectroscopy measurement apparatus (colour online)

3. Results and discussion

In this article, the device under focus is made by depositing two ytterbium contacts onto the surface of a p −type Si wafer to form Yb/p −Si/Yb (abbreviated as YSY). The schematic of the device is shown as an inset in Fig. 2 (a). The figure also illustrates the energy band diagram of the device. The theoretical design takes into account that the electron affinity and work function of p −Si exhibit values of $q\chi_{p-Si} = 4.10$ eV [7] and $q\phi_{p-Si}$=4.97 eV [8]. As the metal work function of ytterbium ($q\phi_{Yb}$ =2.51 eV [9]) is less than the work function of p −Si a Schottky contact is formed at both side of the Yb/p −Si interfaces [10]. At the interface region the bands bend by lowering the vacuum level of material energy band diagram happening on the Yb metal side. The vacuum level is lowered to achieve an equilibrium state of charge carrier distributions at the Fermi level which is close to the valence band of the p −Si. In this process electron diffuses from Yb side to p −Si sides and holes diffuse from p −Si into Yb surface resulting in formation of a space charge region (Schottky barrier of height $q\phi_b$) at the Yb/p −Si interface [10]. $q\phi_b$ blocks the flow of charge carriers across the interface and creates an electric field that

opposes the flow of electrons from Yb to p −Si. Assuming an energy band gap value of 1.18 eV [9], the flat band barrier height of the Yb/p-Si Schottky diode is $q\phi_b = E_g + q\chi_{p-Si} - q\phi_{Yb}$=2.77 eV. The built-in potential is $qV_{bi-1\,or-2} = q\phi_{p-Si} - q\phi_{Yb} = 2.46$ eV. Since the constructed YSY devices are of BBS type one may expect a maximum $qV_{bi} = qV_{bi1} + qV_{bi2}$= 4.92 eV. Forward biasing of one side decreases the built-in potentials (qV_{bi1}) at that side and increases the built-in potential (qV_{bi2}) at the other side to keep charge neutrality and continuity of the electric field within the device [10].

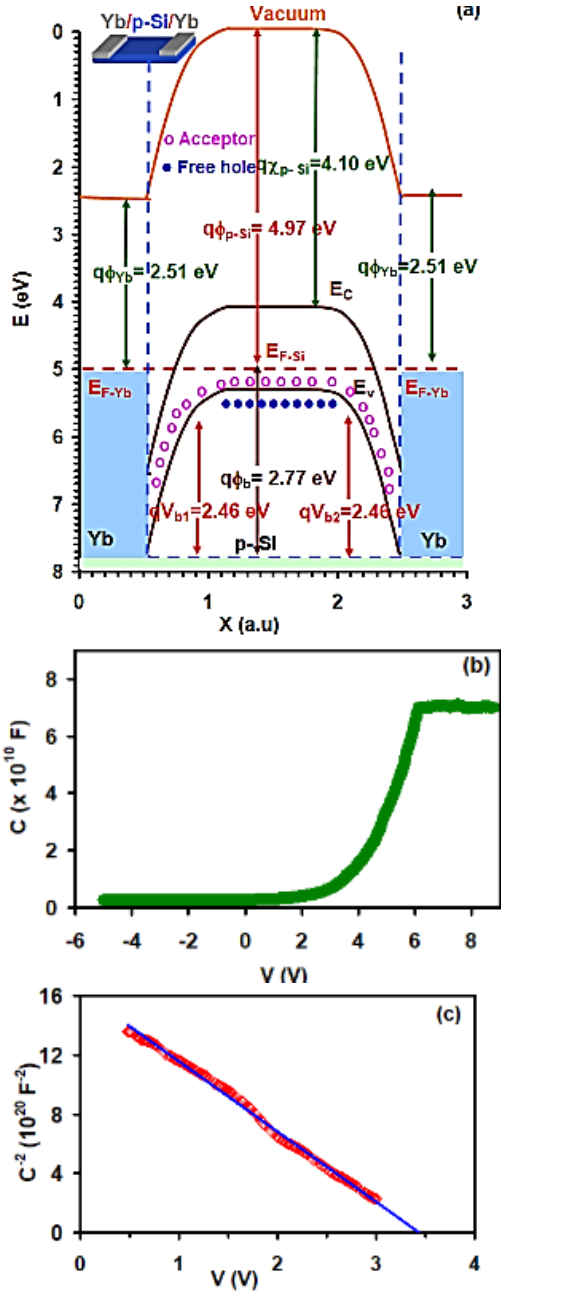

Fig. 2. (a) The schematic and qualitatively band diagram, (b) the capacitance-voltage characteristics measured in the dark and (c) $C^{-2} - V$ representing the abrupt depletion region analyses for MOS type Yb/p-Si/Yb Schottky devices. The inset of (a) shows the schematic of the device (colour online)

Fig. 2 (b) shows the capacitance (C)-voltage (V) characteristic curve for YSY devices. The imposed ac signal frequency was 1.0 MHz. No depletion capacitance can be seen under reverse biasing condition. However, as the forward biasing voltage exceeds 3.15 V, the capacitance sharply increases with increasing forward biased voltage showing a switching from low capacitance to high capacitance mode. The response of the capacitance to the applied voltage is a feature of metal –oxide-semiconductor (MOS) device [10]. As seen from the figure applying positive voltage larger than 3.15 V onsets the depletion capacitance. Under forward biasing conditions the width of the depletion region (w) at the interface narrows because majority carriers or holes are repelled from the Yb metal surface by the positive voltage. They then move deeper into the p-Si layer reducing the extent of the depletion region [9], [12]. When the positive applied voltage increases further ($V > 6.0$ V in Fig. 2 (b)) it attracts the electrons from Yb into p-Si creating an accumulation region. In this case excess minority charge carriers or electrons do exist next to the metal contacts. On the other hand, applying a reverse voltage to the metal widens the depletion region at the interface between Yb and p −Si because holes existing in p −Si are attracted by the negative voltage existing on the metal side. If a sufficiently large negative voltage is applied so that minority carriers or electrons are attracted to the surface of p −Si, they form a conductive channel or layer beneath the metal contact and the device is in the inversion mode and perform as if it was NMOS capacitor [9].

In other words, although the contacts are symmetric, the capacitance values under reverse biasing conditions is much lower than under forward biasing conditions. One explanatory reason is the operation under the reach through condition. In the case of, under reach-through conditions in a semiconductor device, such as a diode, the depletion region extends across the entire width of the device, leading to a significant reduction in the capacitance. Reach-through occurs when the applied voltage is high enough to fully deplete the semiconductor material, causing the depletion region to span from the p-type to the n-type regions, effectively creating a conducting path across the device. In this state, the majority of charge carriers are depleted from the semiconductor, resulting in a sharp decrease in the capacitance. This is because the capacitance is directly related to the charge stored in the depletion region, and with the region fully depleted, the capacitance approaches its minimum value. As a result, under reach-through conditions, the capacitance of the device is significantly reduced compared to when the device is operating in its normal mode [10].

Considering the $C - V$ characteristics in the range of 3.15-6.29 V and assuming an abrupt approximation of the depletion capacitance it was possible to determine the built in potential and effective carrier density, $\widetilde{N}=\frac{N_a N_d}{N_a+N_d}$, where N_a and N_d acceptor and donor concentrations, respectively [9]. The depletion capacitance in accordance with the abrupt approximation is given by the relation [9],

$$C^{-2} = 2\left(V_{bi} - V - \frac{2kT}{q}\right)/(qA^2\varepsilon_\infty\varepsilon_o\widetilde{N}) \qquad (1)$$

Here A=0.0314 cm^2 is the diode area, ε_o is the vacuum dielectric constant and $\varepsilon_\infty = 11.7$ is the high frequency effective dielectric constant [8]. The linear fit of the $C^{-2} - V$ variation shown in Fig. 2 (c) reveal a slope and intercept that allowed determining qV_{bi} and $\widetilde{N}$ values of 3.43 eV and 3.76× 10^{13} cm^{-3}, respectively. The experimentally determined values of qV_{bi} are less than that of the one calculated assuming flat band approximation during the construction of the band diagram where a built-in potential value of $qV_{bi} = qV_{b1} + qV_{b2}$ =2.46+2.46=4.92 eV was determined. The difference is mainly ascribed to the biasing of the devices because forward biasing means reduction of the value of qV_{b1} from its original value (2.46 eV). A forward biasing voltage of 2.46 V cancels V_{b1}keeping $V_{bi} = V_{b2}$. Reverse biasing of the device with 2.46 V cancels V_{b2} making $V_{bi} = V_{b1}$. Also supplying an applied voltage of 2.0 V to the device from one side reduced V_b from 4.92 V to 2.92 V. Other reasons which account for the lower built in potential values include presence of defects [14] and contact resistance [9]. Other devices exhibiting built in potential values of ~3.4 eV were used for the fabrication of light emitting diodes [15]. They are also used in the design of avalanche type field effect transistors [16].

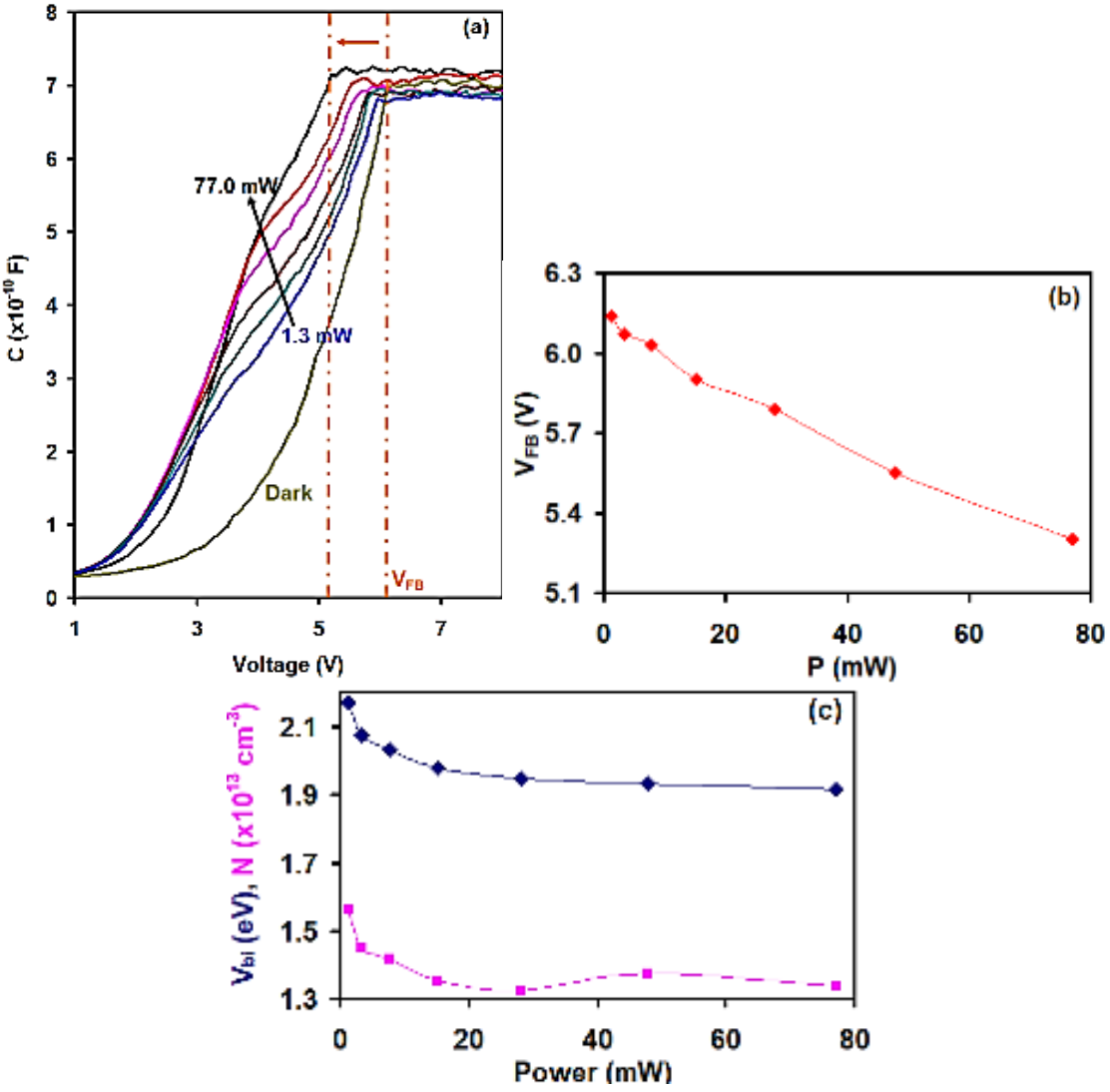

Fig. 3. (a) The illuminated $C - V$ characteristic curves and the light power dependence of (b) the flat band voltage and (c) built in potential and reduced charge density (colour online)

4. Photo-MOS device characteristics

In this section we show the possible control of the YSY MOS device by light illumination. The samples under study were exposed to a mini tungsten lamp used in vehicles. This lamp emits photons in the visible and infrared ranges of light (350-1000 nm [17]). The light power was changed in the range of 1.30-77.0 mW. The measured capacitance-voltage characteristics are shown in Fig. 3 (a). Once again, an ac signal of frequency of 1.0 MHz and of low amplitude (0.10 V) was imposed between the terminals of the device. It is evident from the figure that the capacitance values

increase with increasing light power indicating the high photosensitivity of the capacitance to the light signal. As for examples at an applied forward voltage of 5.0 V the capacitance increased from 376 pF to 466 pF and reaches 673 pF as the light power increased from 0.0 mW to 1.3 mW and reaches 77.0 mW, respectively. In addition, the onset-voltage of the depletion capacitance shifted toward lower values. Consistently the flat-band voltage shown by dashed and dotted orange-colored lines in Fig. 3 (a) (flat band voltage:V_{FB}: the voltage at which the capacitance become voltage invariant) shifted toward lower voltage values. It means that there is a possibility of engineering of the device operation parameters via light power. Fig. 3 (b) and (c) show the power dependencies of the flat band voltage, built in potential and effective charge concentration, respectively. It is evident from Fig. 3 (b) that the flat band voltage decreased linearly with increasing light power reaching a value of 5.3 V at light power of 77 mW. V_{FB} is an important parameter in MOS and MOSFET (MOS field effects transistors) devices because it is directly related to the threshold voltage which is the voltage needed to induce channel formation in the device forcing it to operate in the "ON" or "OFF" mode [9]. Consistent with the behavior of the flat band voltage, the built-in potential also decreases with increasing excitation light power. The decrease in qV_{bi} is associated with a decrease in the value of the reduced carrier concentration (Fig. 3 (c)). One reason for the decrease in the built-in potential and /or flat band voltage with increasing light power is the generation of electron–hole pairs under photo-excitation [18]. These pairs cause a reduction in the built-in electric field within the YSY device which in turn reduces the values of V_{FB} and qV_{bi} [18].

In order to observe the ability of the YSY device to respond to microwave signals, the device was imposed between the terminals of an Agilent dielectric material test fixture (16453A) connect to an impedance analyzer generating driving signals in the frequency (f) domain of 0.01-1.80 GHz. The schematics of the experimental setup together with the photograph of the test fixture are also shown in inset-1 of Fig. 4 (a). The amplitude of the generated signal was kept at the minimum. The measured dark and illuminated capacitance spectra are shown in Fig. 4 (a). It is evident from the figure that the capacitance slowly decreases with increasing driving signal frequency in the domain of 0.01-1.27 GHz. As seen from the enlargement of the $C-f$ variation (inset-2 of Fig. 4 (a)) in the frequency domain of 0.01-1.0 GHz, the illuminated capacitance exhibited larger values than those measured in the dark. In the frequency domain of 1.27-1.80 GHz, the capacitance sharply decreased with increasing driving signal frequency. The decrease in that frequency domain reached two orders of magnitude. No effect of light illumination is seen in in the range of 1.27-1.80 GHz. The capacitance decreased with increasing frequency because of the continuous distribution of the interface states [2,19]. At high frequencies, the charged particles located at the interface struggle to keep up with the rapidly changing ac electric field. Thus, they do not contribute to the capacitance [19,20]. The photocapacitance shown in inset-2 of Fig. 4 (a) refers to the change in capacitance of a semiconductor material when exposed to light arises from an increase in the space charge due to photoemission of charge carriers from a deep defect level located in the depletion region [21]. The loss of the photocapacitance effect observed above 1.0 GHz is ascribed to the transfer of the photo-excited charge carriers back to the original levels or states [22].

Fig. 4 (b) shows the resistance (R) and the magnitude of inductance (L) spectra recorded for the YSY devices. It is evident from the figure that in the frequency domain of 0.01-1.53 GHz, the resistance and inductance of the devices decreases with increasing signal frequency. In the frequency domain of 1.53-1.80 GHz, the resistance and inductance increase with increasing driving frequency. In the frequency range of 0.01-0.47 GHz, the device's resistance under light illumination is higher compared to that in the dark, for a given frequency. However, in the 0.48-1.80 GHz range, the influence of light on resistance disappears, with the resistance values under both light and dark conditions being identical. Regardless of light effect, the decreased values of resistance with increasing signal frequency in the frequency domain of 0.01-1.53 GHz means increased value of conductivity with increasing signal frequency ($\sigma = L/(RA)$; L distance between electrodes and A is the diode area). This trend of variation is usually results from the current transport by the correlated barrier hopping (CBH) [23]. On the other hand, the increase in the resistance value upon photo-excitation can be attributed to generation of charge carriers and formation of localized charge centers. In this process the trapping of light generated- electrons and holes by defects leads to the charge inhomogeneity. Charge inhomogeneity results in a decreased free charge carriers and hence decreased current value [24].

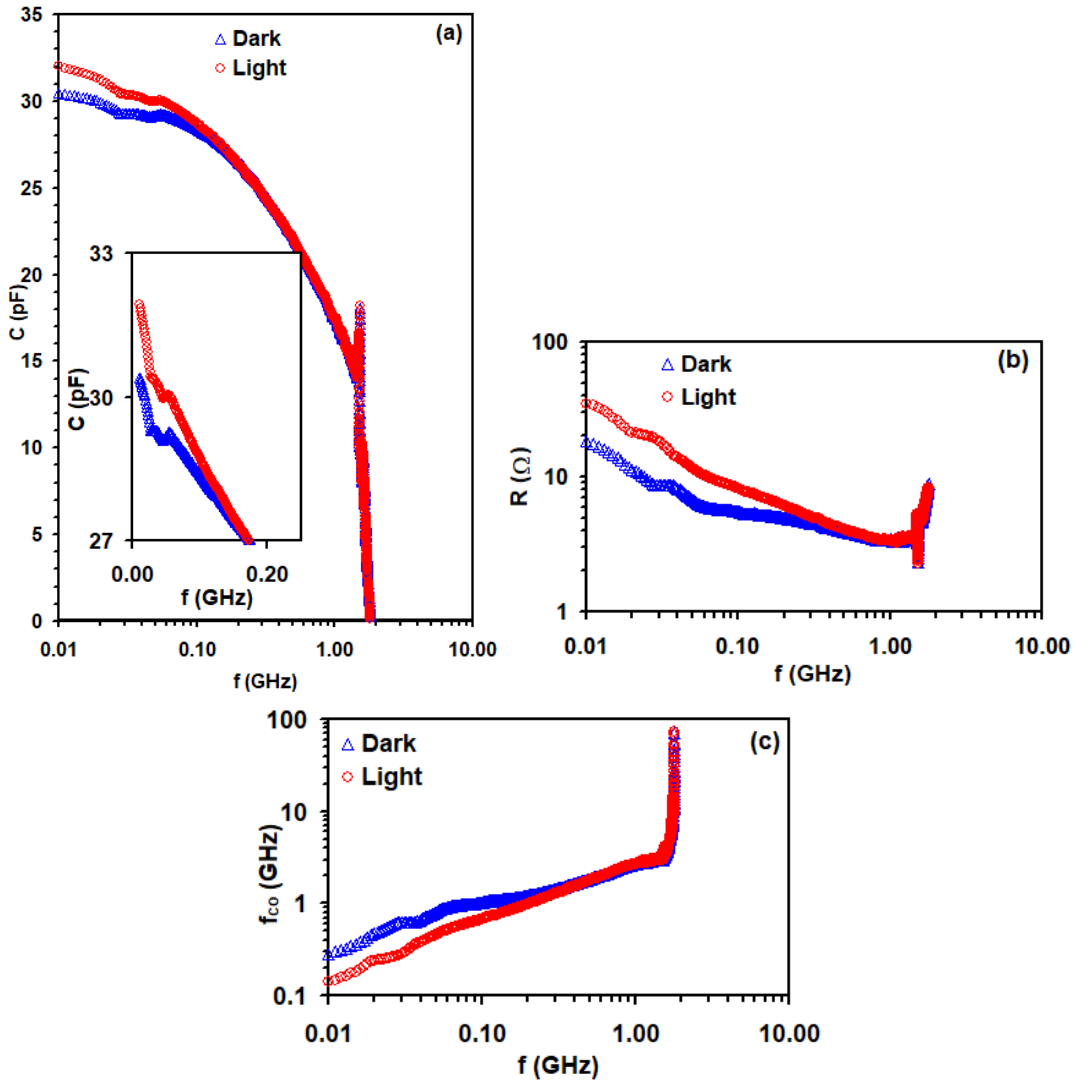

Fig. 4. (a) The capacitance, (b) the resistance and magnitude of inductance and (c) the cutoff frequency spectra for Yb/p −Si/Yb BBS diodes (colour online)

It is worth noting that the cutoff frequency is the frequency at which the signal response of a filter is attenuated by a certain amount. It defines the frequency range over which the filter passes signals with minimal attenuation or loss. It is used by engineers to characterize the performance and bandwidth of a filter, helping to determine its suitability for specific applications [25]. On the other hand, S_{11} parameter is a scattering parameter that represents the magnitude of the reflected signal relative to the incident signal at a specific frequency. It describes how well a filter or other device matches the impedance of the connected system [26]. A low S_{11} value indicates minimal reflection, meaning the device effectively transfers power without significant loss due to reflection. It is used by engineers to assess the performance of filters, antennas, and other components in RF and microwave systems, ensuring efficient signal transmission and reception [27,28].

Fig. 4 (c) shows the experimental cutoff frequency ($f_{co} = (2\pi RC)^{-1}$) spectra for the YSY devices. The cutoff frequency increases smoothly with increasing driving signal frequency in the frequency domain of 0.01-1.45 GHz. In the higher range of frequency domain, the cutoff frequency sharply increases showing values larger than 10 GHz and reaches 1.0 THz as the driving signal frequency exhibit values of 1.55 GHz and 1.7 GHz and 1.80 GHz, respectively. Cutoff frequency drops under illumination inthe frequency domain of 0.01-1.45 GHz. The cutoff frequency decreased upon illumination due to the increase in the capacitance and increase in the resistance under light.

It is important to attract the attention to the values of f_{co} shown in Fig. 4 (c). It indicates that the cutoff frequency can vary in the range of ~0.10 GHz to 3.5 GHz as f increases from 0.01-1.4 GHz. This range of limiting frequency is suitable for 4G/5G technology applications [29], [30]. As for examples, the YSY devices with these limits can fit well with dual port MIMO (multiple input-multiple output) antennas which display resonant band in the range of 3.0-4.20 GHz [31]. This class of antennas was employed in the "fifth-generation new radio n77/n78 sub-6 GHz wireless applications band" [31]. It is also important to recall that the cutoff frequency domain larger than 10 GHz is highly attractive for 6G technology applications

[32]. A maximum inherent cutoff frequency of value of 50-75 GHz was defined for "Millimeter assisted wave technologies in 6G assisted wireless communication systems" [33,34]. Beyond these limits, the ability of the proposed YSY devices to reach 1.0 THz at driving frequency of 1.80 GHz are an additional feature nominating it for use in terahertz technology applications [35,36]. Previous studies have indicated the potential fabrication of a novel category of electronic devices with a cutoff frequency figure-of-merit surpassing few terahertz. These devices demonstrate notable characteristic including high conductance. Such attributes position them as promising candidates for the next generation of ultrafast semiconductor devices [34]. In contrast, the straightforward structure of the YSY BBS devices renders them well-suited for terahertz technology applications.

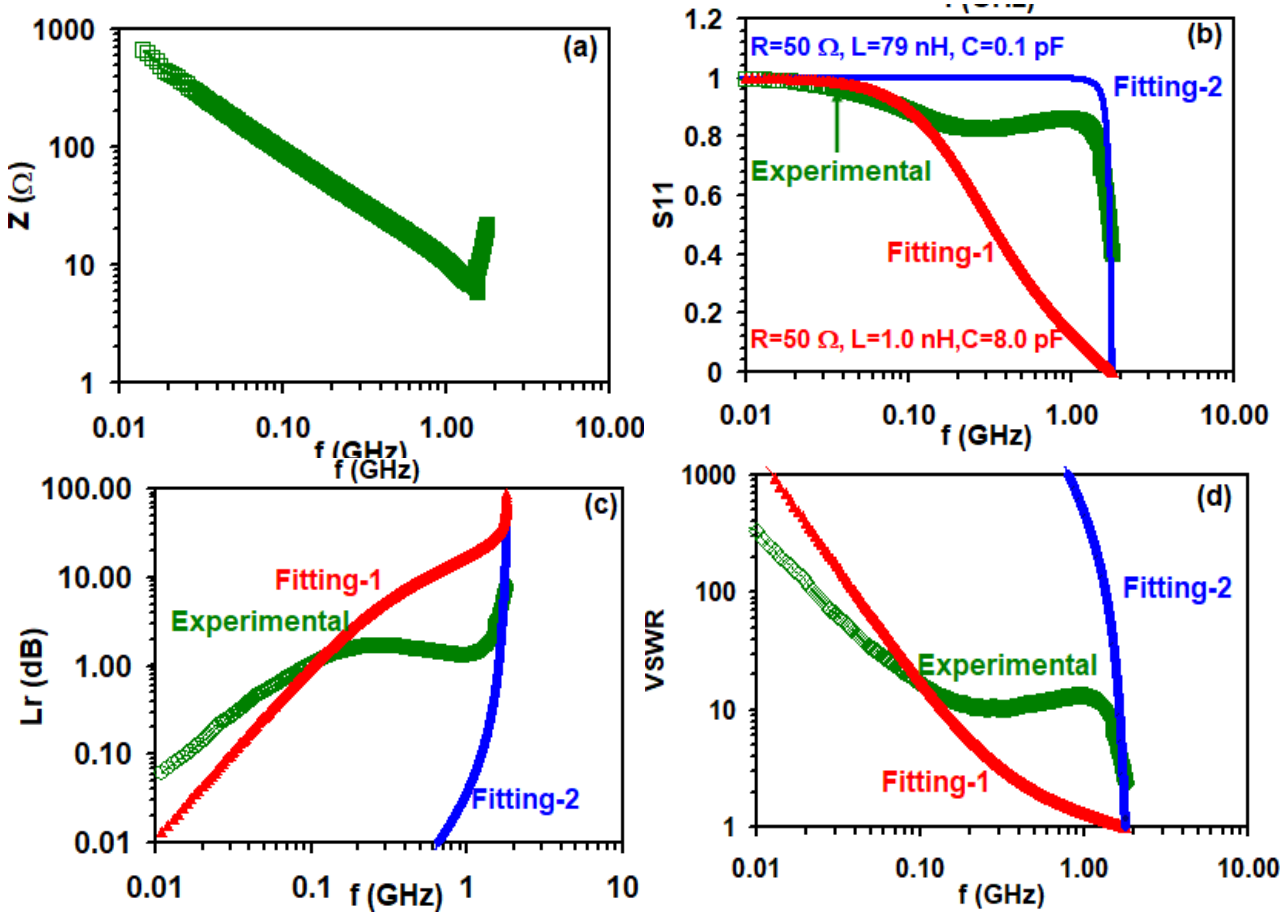

Fig. 5. (a) The impedance, (b) the reflection coefficient, (c) the return loss, and (d) the voltage standing wave ratios for the YSY diodes (colour online)

One practical test of the YSY device was achieved via the dark measurements of the impedance (Z), the magnitude of the reflection coefficient ($S_{11} = \frac{Z_1-1}{Z_1+1}$; $Z_1 = \frac{Z_{YSY}}{Z_{Source}}$ [37]), the return loss ($L_r = -20\log(S_{11})$ [37]) and the voltage standing wave ratios ($VSWR = \frac{1+S_{11}}{1-S_{11}}$ [37]). The respective parameters are presented in Fig. 5 (a), (b), (c) and (d). It is seen from Fig. 5 (a) that the impedance decreases with increasing signal frequency in the frequency domain of 0.01-1.55 GHz. For larger applied frequency values, the impedance switches to high impedance mode. On the other hand, as seen from Fig. 5 (b) the reflection coefficient the so called "S_{11} parameter" measures the amount of electromagnetic energy reflected back from a device relative to an incident energy from a source. Values of $S_{11} = 0$ correspond to maximum and ideal signal transmission while S_{11}=1.0 corresponds to complete rejection of incident signal [37,38]. For the YSY device in accordance with Fig. 5 (b) $S_{11} = 0.38$ is achieved at a driving frequency of 1.80 GHz. More than 60% of the arriving signal is passed at this critical frequency. Assuming that the YSY structure represents an RLC (resistance (R)-inductance (L)-capacitance (C)) circuit connected in series, then the impedance is given by [37],

$$Z_{Device} = R + j\omega L + \frac{1}{j\omega C}\ ,\ \omega = 2\pi f \qquad (2)$$

In accordance with this relation the magnitude of the impedance of the device under study is given by the relation,

$$Z_{Device} = \sqrt{R^2 + (\omega L - (\omega C)^{-1})^2} \qquad (3)$$

Here Z_{Device} is simply Z_{YSY} discussed in the previous paragraph. The equations here assumes that the device has resistance R, inductive reactance $X_L = \omega L$ and capacitive reactance $X_C = 1/(\omega C)$. Following the same rules to calculate S_{11}, L_r and $VSWR$ parameters theoretically it was possible to reproduce the experimental data. Mathematically when $|X_L| = |X_C|$ necessary means $S_{11} = 0$ values is reached. Under these conditions no reflections of the signal at the input port of the device meaning that all of the signal is absorbed or transmitted [39]. It could also be thought that the phase angle between X_L and X_C is $\pm\pi/2$ and the device reached a balanced state where the inductive and capacitive reactances cancel each other out, resulting in a purely resistive impedance [37], [40].

Exact fitting of the experimental data of S_{11} spectra which are shown in Fig. 1 (b) using Eq. (3) was possible with data shown in Table-2. The fitting procedure takes into account the possible values of L and C that suits standard value of R which is usually 50 Ω. The first fitting considers lowering of the resistance to 50 Ω, keeping the experimental value of inductance and determining C value. The second fitting procedure fixes the resistance at a standard of 50 Ω and adapts the value of L and C. Experimentally, for this system the return loss reaches ~8.4 dB at 1.80 GHz. The lowest experimentally determined $VSWR$=2.22 was achieved at 1.80 GHz. As shown in Fig. 5 (d), recalling that L_r measures the electromagnetic power that was not absorbed by the YSY device and thus returned to the source, then the higher the L_r values are the better for signal transmission, the more data transferred. In addition, as the $VSWR$ represents a common measure of the goodness or quality of the match between device and source $VSWR = 1.0$ means ideal matched lines are achieved. From simulation point of view, it is evident from the tabulated data that the high resistance of the device is a main reason for the partial loss of the device quality. In an attempt to guess the ideal R, L, C values of the device so that it shows perfect performance we have carried out a simulation for Eq. (2), the results are shown in Table 2. In accordance with the simulation results presented by red colored fitting "fitting-1", which targets reducing the series resistance value of the device, the reduction of the resistance to 50 Ω can raise the return loss values to 50.4 dB and reduces the S_{11} and $VSWR$ to 0.003 and 1.01, respectively. Reduction of series resistance can be reached by physical modifications like post annealing or parallel resistance connections. Here, the simulation results show that the device can work ideally by connecting a parallel capacitor of 3.0 pF without altering the inductance. Alternatively, with another simulation restriction defined by keeping the resistance at 50 Ω and increasing the inductance by external connections to 79 nH with series connection of a capacitance of 0.10 pF can result in the ideal fitting shown by blue colored line in Fig. 5 (b), (c) and (d). The calculated experimental and simulated parameters of the YSY devices indicate the practical application of the device as band filter operating in the high frequency domain. The tabulated data here are consistent with those reported for coplanar waveguides fed "OM" shaped antenna designed for Quad-band wireless applications [41,42].

Table 2. The YSY microwave resonator parameters designed for high frequency applications

Data	R (Ω)	L (nH)	C (pF)	S_{11}	L_r (dB)	VSWR
Experimental	500	1.0	5.0	0.38	8.4	2.22
Fitting-1	50	1.0	8.0	0.003	50.4	1.01
Fitting-2	50	79	0.1	0.002	54.0	1.00

*Values of S_{11}, L_r and $VSWR$ are listed for signal subjected to driving frequency of 1.80 GHz

It is worth mentioning that the results reported in this work indicate the advantages of the YSY structure compared to other similar structures. In a similar study Yb/SiO_2/Si tunneling devices exhibited transition from MOS to Schottky contact as the oxide layer thickness is increased [43]. The device showed very high contact resistance that was lowered based on oxidation temperature [43]. Oxidation effect is absent in YSY devices resulting in high stability device performance with no additional contact resistance effect. In another work well performing MOS devices made of $ZrTiO_4$/Yb_2O_3 showed flat band voltage of -1 V and demanded as long-life time operating device [44]. However, these devices need annealing at 800 °C to be constructed [44]. The preparation of YSY devices is easier and need no additional issue other than deposition of metals. In another similar work, Yb/MoO_3/Yb MOS devices exhibited microwave device characteristics but the return loss values being 26 dB for this device are much lower than that of YSY devices where value of ~50 dB is recorded [45]. For future optoelectronic applications further electronic and optical insights like light illuminated thermally stimulated current of positive and negative contacts need to be considered [46,47]. In addition, some measurements on the photoluminescence spectrum are needed to explore the impurity and defect states on the recombination dynamics of the device. Reduction of defects will improve the photosensitivity of the device [47,48]. In the same context, visualization of trap distribution through trap spectroscopy by charge injection and sensing will provide a possibility to enhance Yb/Si/Yb interface properties [49,50]. These enhancements will open the doors toward the design of branch line couplers on Si substrates performing as resonator workable above 5.0 GHz [51,52]. Enhancement of interface properties and construction of multi-couplers on the same substrate will enable multiple communication

systems to complement radio resources in 6G systems [53], [54].

5. Conclusions

In the current work, we have shown that two metal contacts of ytterbium (Yb) onto p-type Si substrates can operate as a back-to-back Schottky device. The device functions as a metal-oxide-semiconductor (MOS) capacitor whose electrical properties can be effectively tuned under light illumination. Dark measurements of the capacitance–voltage (C–V) characteristics revealed the formation of a built-in potential of 3.43 eV, which decreases with increasing light intensity, indicating that the device output can be easily engineered by exposure to visible light from a miniature tungsten lamp. Impedance spectroscopy analyses demonstrated that the device operates as a high-frequency microwave band filter, exhibiting a photo-controlled cutoff frequency ranging from 0.10 GHz to over 50 GHz. Under microwave excitation at 1.80 GHz, the device showed a reflection coefficient (S_{11}) of 0.003, a return loss of 50.4 dB, and a voltage standing wave ratio of 1.01 when resistance and capacitance were optimized to 50 Ω and 8.0 pF, respectively. These high-performance metrics make the Yb/p-Si/Yb device structure a strong candidate for 6G and terahertz applications.

Acknowledgements

This project was funded by the Deanship of Scientific Research (DSR) at Arab American University, Jenin, Palestine and by Istinye University, Istanbul, TR. The authors therefore acknowledge both institutes with thanks.

References

[1] R. Fukumori, T. Xie, A. Faraon, CLEO 2023, Technical Digest Series, San Jose, CA, FTh4A.3 (2023).
[2] O. Sinitskaya, K. Shubina, A. Vorobyev, S. Timoshnev, E. Nikitina, Y. Enns, International Conference on Electrical Engineering and Photonics (EExPolytech), 279 (2023).
[3] D. A. Aldemir, M. Kaleli, A. C. Yavru, Sensors and Actuators A: Physical. **311**, 112091 (2020).
[4] A. F. Qasrawi, R. B. Daragme, Journal of Ovonic Research **18**(2), 253 (2022).
[5] H. E. Lapa, A. Kökce, D. A. Aldemir, A. F. Özdemir, Journal of Materials Science: Materials in Electronics **32**(4), 4448 (2022).
[6] H. E. Lapa, Ç. Ş. Güçlü, D. A. Aldemir, A. F. Özdemir, Applied Physics A **126**(6), 473 (2020).
[7] S. Cao, J. Li, J. Zhang, Y. Lin, L. Lu, J. Wang, M. Yin, L .Yang, X. Chen, D. Li, Advanced Functional Materials **30**(49), 2004367 (2020).
[8] S. E. Algarni, A. F. Qasrawi, N. M. Khusayfan, Silicon **16**(6), 2341 (2024).
[9] A. F. Qasrawi, R. B. Daragme, Physica Status Solidi A, **219**(18), 2100822 (2022).
[10] S. M. Sze, Y. Li, K. K. Ng, Physics of Semiconductor Devices, John Wiley & Sons, 2021.
[11] Jyoti, R. Pandey, N. S. Raghava, Microsystem Technologies **29**(6), 875 (2023).
[12] S. J. Moxim, F. V. Sharov, D. R. Hughart, G. S. Haase, C. G. McKay, E. B. Frantz, P. M. Lenhan, Review of Scientific Instruments **93**(11), 4 (2022).
[13] J. T. Penttinen, The LTE-Advanced Deployment Handbook: The Planning Guidelines For The Fourth Generation Networks, John Wiley & Sons, 2016.
[14] U. K. Verma, A. Singh, International Journal of Convergence in Healthcare **3**(2), 55 (2023).
[15] E. Jung, J. K. Lee, M. S. Kim, H. Kim, IEEE Transactions on Electron Devices **62**(10), 3322 (2015).
[16] J. Liu, M. Xiao, R. Zhang, S. Pidaparthi, H. Cui, A. Edwards, M. Craven, L. Baubutr, C. Drowley, Y. Zhang, IEEE Transactions on Electron Devices **68**(4), 2025 (2021).
[17] G. E. Ratto, F. A. Videla, J. H. M. Valdiviezo, Proceedings of Spie **11814**, 110 (2021).
[18] C. Chen, J.-M. Hwang, Y.-W. Ok, W.-J. Choi, V. Upadhyaya, B. Rounsaville, A. Rohatgi, Journal of Applied Physics **132**(21), 213302 (2022).
[19] A. Mekki, R. O. Ocaya, A. Dere, A. A. Al-Ghamdi, K. Harrabi, F. Yakuphanoglu, Synthetic Metals **213**, 47 (2016).
[20] Y. S. Ocak, Journal of Alloys and Compounds **513**, 13 (2012).
[21] A. M. Armstrong, A. A. Allerman, Applied Physics Letters **111**(4), 042103 (2017).
[22] I. A. Elsayed, M. Çavaş, R. Gupta, T. Fahmy, A. A. Al-Ghamdi, F. Yakuphanoglu, Journal of Alloys and Compounds **638**, 166 (2015).
[23] E. A. Tutov, A. V. Manannikov, H. I. Al-Khafaji, V. P. Zlomanov, Technical Physics **62**(3), 390 (2017).
[24] A. Ben Gouider Trabelsi, F. V. Kusmartsev, M. B. Gaifullin, D. M. Forrester, A. Kusmartseva, M. Oueslati, Nanoscale **9**(32), 11463 (2017).
[25] B. Cao, J. Zhao, X. Liu, Y. Li, Science China Information Sciences **67**(7), 170306 (2024).
[26] Y. Wang, R. Xiao, N. Xiao, Z. Wang, L. Chen, Y. Wen, P. Li, Advanced Electronic Materials **8**(10), 2200370 (2022).
[27] Y. Yang, Z. Zhang, Y. Zhou, C. Wang, H. Zhu, IEEE Transactions on Microwave Theory and Techniques **71**(2), 907 (2022).
[28] P. Wen, Y. Jiang, F. Liu, Z. Ma, Y. Wang, IEEE Transactions on Circuits and Systems II: Express Briefs **71**(9), 4346 (2024).
[29] J-.H. Choi, H.-S. Kwon, J.-M. Yang, Microwave and Optical Technology Letters **62**(1), 125 (2020).
[30] A. F. Qasrawi, N. M. A. Yaseen, Physica Scripta **96**(12), 125819 (2021).
[31] A. K. Dwivedi, N. K. Narayanaswamy,

K. K. V. Penmatsa, S. K. Singh, A. Sharma, V. Singh, Scientific Reports **13**(1), 13994 (2023).
[32] R. A. Almotiri, A. F. Qasrawi, S. E. Algarni, Physica Scripta **97**(12), 125811 (2022).
[33] M. M. M. Ali, M. Elsaadany, S. I. Shams, K. Wu, IEEE Transactions on Microwave Theory and Techniques **72**(2), 892 (2023).
[34] A. Alam, M. S. Alam, K. AlMuhanna, H. Zhang, A. Shamim, Z. A. Shamsan, IEEE Access **11**, 109539 (2023).
[35] C. Wang, P. Wen, X. Huang, K. Chen, K.-D. Xu, Optics Express **32**(13), 22748 (2024).
[36] S. E. Algarni, A. F. Qasrawi, N. M. Khusayfan, Optical and Quantum Electronics **56**(3), 286 (2023).
[37] D. M. Pozar, Microwave Engineering, Wiley, 2011.
[38] S. E. A. Garni, A. F. Qasrawi, IEEE Transactions on Electron Devices **64**(1), 244 (2017).
[39] P. Wen, Y. Jiang, F. Liu ,C. Wang, Z. Ma, Y. Wang, AEU - International Journal of Electronics and Communications **176**, 155159 (2024).
[40] X.-L. Huang, L. Zhou, M. Völkel, A. Hagelauer, J.-F. Mao, R. Weigel, IEEE Transactions on Microwave Theory and Techniques **66**(12), 5573 (2018).
[41] A. K. Yadav, S. Lata, S. K. Singh, A. K. Singh, T. Sharan, M. N. Masri, Journal of Electronic Materials **52**(7), 4388 (2023).
[42] S. Zha, Z. Qu, J. Zhang, D. Zheng, P. Liu, IEEE Transactions on Antennas and Propagation **72**(9), 7252 (2024).
[43] P. Bauernschmitt, J. Lindolf, U. Kunze, Microelectronic Engineering **22**(1-4), 105 (1993).
[44] Y. Wu, R. Lyu, M. Wu, L. Chen, Ch. Lin, IEEE Electron Device Letters **33**(3) 426 (2012).
[45] S. E. Al Garni, A. F. Qasrawi, Current Applied Physics **19**(5), 639 (2019).
[46] M. Isik, G. Altuntas, N. M. Gasanly, Journal of Electronic Materials **54**, 4101 (2025).
[47] M. Isik, G. Altuntas, N. M. Gasanly, N. H. Darvishov, Materials Letters **383**, 137990 (2025).
[48] Yu, Mubing, T. Qin, G. Gao, K. Zu, D. Zhang, N. Chen, D. Wang, Y. Hua, H. Zhang, Y. B. Zhao, J. Zhu, Light: Science and Applications **14**(1), 102 (2025).
[49] H. Yuan, Y. Huang, T. Gong, Y. Wang, P. Jiang, W. Wei, Yang Yang, Y. Yang, J. Chai, Z. Wu, X. Wang, Q. Luo, IEEE Electron Device Letters **45**(12), 2371 (2024).
[50] Li, Ce, X. Chen, Z. Zhang, X. Wu, T. Yu, R. Bie, D. Yang, Y. Yao, Zh. Wang, L. Sun, Nano Letters **24**(47), 15025 (2024).
[51] Y. Deng, F. Wang, X. Yin, S. Xiao, Y. Yang, N. Yu, IEEE Transactions on Components, Packaging and Manufacturing Technology **15**(3), 623 (2025).
[52] Y. Deng, F. Wang, X. Yin, Y. Yang, N. Yu, Y. Li, IEEE Transactions on Components, Packaging and Manufacturing Technology **15**(1), 165 (2025).
[53] H. Luo, G. Sun, Ch. Chi, H. Yu, M. Guizani, IEEE Wireless Communications **32**(2), 18 (2025).
[54] G. Sun, Zh. Xu, H. Yu, V. Chang, IEEE Transactions on Industrial Informatics **17**(10), 7155 (2020).

*Corresponding author: atef.qasrawi@aaup.edu